PFC/JA-90-34

MULTIMODE INTERACTIONS IN CYCLOTRON AUTORESONANCE MASER AMPLIFIERS

Chiping Chen and Jonathan Wurtele
Department of Physics and Plasma Fusion Center
Massachusetts Institute of Technology
Cambridge, MA 02139

September, 1990

Research supported by the Department of Energy, Office of Basic Energy Sciences, the Department of Energy, High Energy Physics Division, and the Office of Naval Research.

MULTIMODE INTERACTIONS IN CYCLOTRON AUTORESONANCE MASER AMPLIFIERS

Chiping Chen and Jonathan S. Wurtele
Department of Physics and Plasma Fusion Center
Massachusetts Institute of Technology
Cambridge, Massachusetts 02139

ABSTRACT

The interaction of transverse eigenmodes with a relativistic electron beam is analyzed in an overmoded cyclotron autoresonance maser amplifier, using a nonlinear self-consistent model and kinetic theory. It is shown that all of the coupled modes grow with the dominant unstable mode at the same growth rate, but suffer different launching losses. The phases of coupled modes are locked in the linear and nonlinear regimes. Simulations indicate that the rf power distribution among the interacting modes at saturation is *insensitive* to input power distribution but *sensitive* to detuning.

PACS numbers: 42.52.+x, 52.75.Ms, 52.35.Mw

One of the most intriguing problems in the generation of coherent radiation using a relativistic electron beam is the interaction of multiple electromagnetic eigenmodes with the electron beam. In free electron laser (FEL) oscillators[1,2] and gyrotrons,[3] mode competition determines the temporal behavior of the eigenmodes of the cavity and the radiation spectrum. Multimode phenomena also occur in overmoded amplifier systems, where the temporal dependence of the eigenmodes is usually sinusoidal. In such cases, the eigenmodes evolve spatially as a result of the interaction with the electron beam.

A nonlinear multimode theory is indispensable in order to predict the rf power in each mode. Multiple waveguide mode interactions have been investigated using linear theory[4] and computer simulations[5] for FEL amplifiers, but detailed comparisons between theory and simulations are not (yet) available. There have been few theoretical studies of multimode interactions in cyclotron autoresonance maser (CARM) amplifiers[6-11] in waveguide configurations, despite the fact that many planned CARM amplifier experiments will operate in an overmoded waveguide.

In this letter, we present a general treatment of multimode interactions in an overmoded single-frequency CARM amplifier, using a nonlinear self-consistent model and kinetic theory. A complete set of CARM amplifier equations with multiple modes, which are derived from the standpoint of particle-wave interactions (similar to the FEL equations derived by Kroll, Morton, and Rosenbluth[12]), are integrated numerically to calculate the linear and nonlinear evolution of coupled transverse eigenmodes and of the relativistic electron beam. In addition, use is made of the linearized Maxwell-Vlasov equations and the Laplace transform to derive a dispersion relation and amplitude equations for the CARM instability with an arbitrary number of vacuum transverse-electric (TE) and transverse-magnetic (TM) waveguide modes. The Laplace transform analysis allows for analytical calculation of launching losses and the three-dimensional radiation field profile. Although the present treatment is devoted specifically to the CARM amplifier, we believe

that the basic ideas are applicable to a large class of amplifier-type free electron devices including free electron lasers, gyrotron traveling-wave tubes,[13] Cherenkov masers,[14] etc.

We consider the CARM interaction[7,8] of a relativistic electron beam with a co-propagating electromagnetic wave $(\omega, \vec{k})$ in a lossless cylindrical waveguide of radius r_w immersed axially in the uniform magnetic field $B_0\vec{e}_z$. The cyclotron resonance condition is $\omega = k_z v_z + l\Omega_c/\gamma$. Here, v_z and γ are, respectively, the axial velocity and relativistic mass factor of the beam electrons; l is the harmonic number; $\Omega_c = eB_0/mc$ is the nonrelativistic cyclotron frequency; m and $-e$ are the electron mass and charge, respectively; and c is the speed of light *in vacuo*. For simplicity, we present the analysis for the multimode CARM interaction involving an arbitrary number of vacuum TE modes with azimuthal dependence $e^{i\theta}$, maintaining the general features of multimode phenomena (which will be discussed elsewhere[15]).

It can be shown that a complete set of nonlinear equations describing an overmoded CARM amplifier with multiple TE_{1n} modes can be expressed in the dimensionless form[8,15]

$$\frac{d\gamma}{d\hat{z}} = -\frac{\hat{p}_\perp}{\hat{p}_z}\sum_n X_n(r_L, r_g) A_n \cos\psi_n \ , \tag{1}$$

$$\frac{d\hat{p}_z}{d\hat{z}} = -\frac{\hat{p}_\perp}{\hat{p}_z}\sum_n X_n(r_L, r_g)\left[\left(\frac{1}{\beta_{\phi n}} + \frac{d\delta_n}{d\hat{z}}\right) A_n \cos\psi_n + \frac{dA_n}{d\hat{z}}\sin\psi_n\right] , \tag{2}$$

$$\frac{d\psi_n}{d\hat{z}} = \frac{1}{\beta_{\phi n}} + \frac{d\delta_n}{d\hat{z}} - \frac{\gamma}{\hat{p}_z} + \frac{\hat{\Omega}_c}{\hat{p}_z}$$
$$+ \frac{1}{\hat{p}_z\hat{p}_\perp}\sum_{n'} W_{n'}(r_L, r_g)\left\{\left[\gamma - \hat{p}_z\left(\frac{1}{\beta_{\phi n'}} + \frac{d\delta_{n'}}{d\hat{z}}\right)\right] A_{n'}\sin\psi_{n'} + \hat{p}_z\frac{dA_{n'}}{d\hat{z}}\cos\psi_{n'}\right\} , \tag{3}$$

$$\left(\frac{d^2}{d\hat{z}^2} + \frac{1}{\beta_{\phi n}^2}\right) A_n(\hat{z}) \exp\left\{i\left[\frac{\hat{z}}{\beta_{\phi n}} + \delta_n(\hat{z})\right]\right\}$$
$$= \frac{2ig_n}{\beta_{\phi n}}\left\langle X_n(r_L, r_g)\frac{\hat{p}_\perp}{\hat{p}_z}e^{-i\psi_n}\right\rangle \exp\left\{i\left[\frac{\hat{z}}{\beta_{\phi n}} + \delta_n(\hat{z})\right]\right\} , \tag{4}$$

where n is a positive integer and the normalized coupling constant g_n is defined by

$$g_n = \frac{4(\beta_{\phi n}^2 - 1)}{\beta_{\phi n}(\nu_n^2 - 1)[J_1(\nu_n)]^2}\left(\frac{I_b}{I_A}\right) .$$

Equations (1)-(3) describe the dynamics of each individual particle, and Eq. (4) governs the slowly varying wave amplitude $A_n(\hat{z})$ and phase shift $\delta(\hat{z})$ for each TE_{1n} mode. In the simulations, typically, we use more than 1024 particles. In Eqs. (1)-(4), $\hat{z} = \omega z/c$ is the normalized interaction length; $\omega = 2\pi f$ is the angular frequency of the input signal; $\hat{\Omega}_c = \Omega_c/\omega$ is the normalized nonrelativistic cyclotron frequency; $\hat{p}_z = p_z/mc = \gamma\beta_z$, $\hat{p}_\perp = p_\perp/mc = \gamma\beta_\perp$, and $\gamma = (1 + \hat{p}_z^2 + \hat{p}_\perp^2)^{1/2}$ are, respectively, the normalized axial and transverse momentum components, and the relativistic mass factor of an electron; I_b is the beam current; $I_A = mc^3/e \cong 17$ kA is the Alfvén current; $X_n(r_L, r_g) = J_0(k_n r_g)J_1'(k_n r_L)$ and $W_n(r_L, r_g) = J_0(k_n r_g)J_1(k_n r_L)/k_n r_L$ are geometric factors; $J_0(x)$ is the lowest order Bessel function; $J_1'(x) = dJ_1(x)/dx$ is the derivative of the first-order Bessel function; ν_n is the nth zero of $J_1'(x)$; $k_n = \nu_n/r_w$ is the transverse wavenumber associated with the TE_{1n} mode; $\beta_{\phi n} = \omega/ck_{zn} = (1 - c^2k_n^2\omega^2)^{-1/2}$ is the normalized phase velocity of the vacuum TE_{1n} waveguide mode; $r_L = p_\perp/m\Omega_c$ is the electron Larmor radius; r_g is the electron guiding-center radius which is assumed to be constant; $< \cdots >$ denotes the ensemble average over the particle distribution.

The rf power flow over the cross section of the waveguide for the TE_{1n} mode, $P_n(z)$, is related to the normalized wave amplitude A_n by the expression

$$P_n(\hat{z}) = \frac{1}{8}\left(\frac{m^2c^5}{e^2}\right)\frac{(\nu_n^2 - 1)[J_1(\nu_n)]^2}{(1 - \beta_{\phi n}^{-2})}\left(\beta_{\phi n}^{-1} + \frac{d\delta_n}{d\hat{z}}\right)A_n^2(\hat{z}) , \qquad (5)$$

where $m^2c^5/e^2 \cong 8.7$ GW. Equations (1)-(4) are readily solved numerically to yield the three-dimensional radiation field profile and the distribution of rf power among coupled

modes in the multimode CARM interaction. For the simulation results presented below, the particles are loaded such that the right-hand side of Eq. (4) vanishes at $z = 0$, corresponding to an initially unbunched electron beam.

By performing the Laplace transform of the linearized Maxwell-Vlasov equations, a dispersion relation and amplitude equations can be derived for the multimode CARM interaction, with an arbitrary number of vacuum TE and TM waveguide modes coupling to the electron beam. For example, applying our results to the coupling of a cold, thin ($k_n r_g \ll 1$), azimuthally symmetric electron beam with the TE_{1n} modes at the fundamental cyclotron frequency ($l = 1$), and assuming $dE_n(0)/dz = 0$, the Laplace transform of the equations for the amplitudes $E_n(z) \sim A_n(z)\exp[ik_{zn}z + \delta_n(z)]$ to leading order in $c^2k_n^2/(\omega - \Omega_c/\gamma - k_z v_z)^2$ can be expressed in the matrix form[15]

$$\left(s^2 - k_n^2 + \frac{\omega^2}{c^2}\right)\hat{E}_n(s) + \sum_{n'=1}^{N} \frac{\epsilon_{nn'}k_{n'}^2(\omega^2 + c^2s^2)}{(\omega - \Omega_c/\gamma + iv_z s)^2}\hat{E}_{n'}(s)$$
$$= sE_n(0) + \sum_{n'=1}^{N} \frac{i\epsilon_{nn'}k_{n'}^2 v_z \omega}{(\omega - \Omega_c/\gamma + iv_z s)^2}E_{n'}(0) \; . \tag{6}$$

In Eq. (6), $s = ik_z$ is the Laplace transform variable; $\beta_z = v_z/c$ and $\beta_\perp = v_\perp/c$ are, respectively, the normalized axial and transverse velocities of the equilibrium beam electrons; ck_N is the largest cut-off frequency below the operating frequency ω; and the dimensionless coupling constants $\epsilon_{nn'}$ are defined by

$$\epsilon_{nn'} = \frac{4\beta_\perp^2}{\gamma\beta_z}\left(\frac{I_b}{I_A}\right)\frac{X_n(r_L, r_g)X_{n'}(r_L, r_g)}{[(\nu_n^2 - 1)(\nu_{n'}^2 - 1)]^{1/2}J_1(\nu_n)J_1(\nu_{n'})} \; .$$

Therefore, the amplitudes $E_n(z)$ and the dispersion relation can be obtained by solving Eq. (6) and performing the inverse Laplace transform of $\hat{E}_n(s)$.

For two coupled modes, TE_{1n} and $TE_{1n'}$, it is readily shown from Eq. (6) that the dispersion relation is

$$\left(k_z^2+k_n^2-\frac{\omega^2}{c^2}\right)\left(k_z^2+k_{n'}^2-\frac{\omega^2}{c^2}\right)\left(\omega-\frac{\Omega_c}{\gamma}-k_z v_z\right)^2$$

$$= \left[\epsilon_{nn}k_n^2\left(k_z^2+k_{n'}^2-\frac{\omega^2}{c^2}\right)+\epsilon_{n'n'}k_{n'}^2\left(k_z^2+k_n^2-\frac{\omega^2}{c^2}\right)\right](\omega^2-c^2k_z^2)\ . \qquad (7)$$

When the two modes are well separated and $\epsilon_{nn}k_n^2(k_z^2+k_{n'}^2-\omega^2/c^2) \gg \epsilon_{n'n'}k_{n'}^2(k_z^2+k_n^2-\omega^2/c^2)$, corresponding to the beam cyclotron mode, $\omega = k_z v_z + \Omega_c/\gamma$, in resonance with the TE_{1n} mode, $\omega = c(k_z^2+k_n^2)^{1/2}$, the coupled-mode dispersion relation in Eq. (7) becomes the usual single-mode dispersion relation[8,9]

$$k_z^2+k_n^2-\frac{\omega^2}{c^2}=\frac{\epsilon_{nn}k_n^2(\omega^2-c^2k_z^2)}{(\omega-\Omega_c/\gamma-k_z v_z)^2}$$

for the TE_{1n} mode.

Typical results from the computer simulations and kinetic theory are summarized in Figs. 1-3. Figure 1 shows the dependence of rf power, in the TE_{11} and TE_{12} modes, on the interaction length z for (a) single-mode CARM interactions and (b) the CARM interaction with both modes coupling to the beam. The system parameters in Fig. 1 are beam current $I_b = 500$ A, beam energy $E_b = 1.0$ MeV ($\gamma = 2.96$), initial pitch angle $\theta_{p0} = \beta_{\perp 0}/\beta_{z0} = 0.6$, waveguide radius $r_w = 2.7$ cm, and axial magnetic field $B_0 = 3.92$ kG, corresponding to the TE_{11} mode in resonance, and the TE_{12} mode off resonance, with the electron beam. The solid curves are the simulation results obtained by integrating numerically Eqs. (1)-(4) with 1024 particles; The dashed curves are obtained analytically from Eq. (6). The inclusion of the coupling of the TE_{11} and TE_{12} modes results in instability for the TE_{12} mode as seen in Fig. 1(b), while the single-mode theory predicts complete stability for the TE_{12} mode as seen in Fig. 1(a). In fact, in Fig. 1(b), the TE_{12} mode grows parasitically with the dominant unstable TE_{11} mode, and the two coupled modes have the same spatial growth rate $-\mathrm{Im}\Delta k_z > 0$, corresponding to the

most unstable solution of the dispersion relation in Eq. (7). Because the TE_{11} mode is in resonance with the beam mode and the TE_{12} mode is detuned from resonance, the TE_{12} mode suffers greater launching losses than the TE_{11} mode.

The simulation also shows that the relative rf phase $\Delta\phi(z) = (k_{z2} - k_{z1})z + \delta_2(z) - \delta_1(z)$ for the coupled modes is approximately constant in the exponential gain regime. Such a phase-locking phenomenon is expected from linear theory, because the dispersion relation in Eq. (7) yields a unique solution of k_z with a negative imaginary part, which determines the spatial growth rate and phase shifts for both modes in the exponential gain regime. What is remarkable is that phase locking persists even in the nonlinear regime, at least for some finite interaction length after saturation. This reveals two general features of the multimode CARM interaction: (1) all of the coupled modes have the same growth rate, but suffer different launching losses which depend upon detuning characteristics; (2) the phases of coupled waveguide modes are locked in the exponential gain regime, and remain locked for some finite interaction length after saturation.

Another interesting feature of the multimode CARM interaction is that the rf power distribution among the coupled modes at saturation is *insensitive* to the small-input rf power distribution at $z = 0$. Figure 2 shows the results of the simulations for the coupling of the TE_{11} and TE_{12} modes with two different distributions of input rf power. In Fig. 2, the two solid curves depict the linear and nonlinear evolution of rf power in the TE_{12} mode obtained from the simulations with the two input rf power distributions: (a) $P_0(TE_{11})$ = 1.0 kW and $P_0(TE_{12})$ = 1.0 kW, and (b) $P_0(TE_{11})$ = 1.0 kW and $P_0(TE_{12})$ = 1.0 W, while the two dashed curves are the corresponding analytical results from Eq. (6). Here, only the TE_{12} mode is plotted because the TE_{11} mode remains virtually unchanged for the two cases.

Figure 3 depicts the detuning characteristics of the saturated rf power distribution among four coupled TE_{1n} modes ($n = 1, 2, 3, 4$), as obtained from the simulation with an

input power of 100 W per mode. By increasing the axial magnetic field B_0 in Fig. 3, the beam mode is tuned through the resonances with the TE_{11}, TE_{12}, TE_{13}, and TE_{14} modes at B_0 = 3.74, 4.29, 5.33, and 6.98 kG, respectively. The fractional rf power for a given mode reaches a maximum at its resonant magnetic field, while the power decreases rapidly for off-resonance modes. In the transition from one resonance to another, however, two adjacent competing modes can have comparable rf power levels at saturation.

In summary, we have presented a general treatment of multimode interactions in an overmoded CARM amplifier using a nonlinear self-consistent model and kinetic theory. Good agreement was found between the simulations and kinetic theory in the linear regime. It was shown analytically, and confirmed in the simulations, that all of the coupled waveguide modes grow with the dominant unstable mode at the same spatial growth rate, but suffer different launching losses which depend upon detuning. Phase locking occurs among coupled waveguide modes in the linear and nonlinear regimes. The saturated rf power in each mode was found to be insensitive to input power distribution, but sensitive to detuning. An accurate calculation of the growth rate and saturation levels in overmoded CARM amplifiers requires the use of a multimode theory in the linear and nonlinear regimes. We believe that the present analysis can be generalized to treat multimode phenomena in various free electron devices.

ACKNOWLEDGMENTS

The authors wish to thank B.G. Danly for helpful discussions. This work was supported by the Department of Energy, Office of Basic Energy Sciences, the Department of Energy, High Energy Physics Division, and the Office of Naval Research.

REFERENCES

1. Ya.L. Bogomolov, V.L. Bratman, N.S. Ginzburg, M.I. Petelin, and

A.D. Yanakovsky, Opt. Commun. **36**, 109 (1981).

2. T.M. Antonsen, Jr. and B. Levush, Phys. Rev. Lett. **62**, 1488 (1989); L. R. Ellis, G. Ramain, J. Hu, and A. Amir, *ibid*, **55**, 424 (1986).
3. K.E. Kreischer and R.J. Temkin, Phys. Rev. Lett. **59**, 547 (1987).
4. E. Jerby and A. Gover, Phys. Rev. Lett. **63**, 864 (1989).
5. R.A. Jong, W.M. Fawley, and E.T. Scharlemann, SPIE Vol. 1045, 18 (1989).
6. G. Bekefi, A. DiRienzo, C. Leibovitch, and B.G. Danly, Appl. Phys. Lett. **54**, 1302 (1989).
7. V.L. Bratman, G.G. Ginzburg, G.S. Nusinovich, M.I. Petelin, and P.S. Strelkov, Int. J. Electron. **51**, 541 (1981), and references therein.
8. A.W. Fliflet, Int. J. Electron. **61**, 1049 (1986).
9. K.R. Chu and A.T. Lin, IEEE Trans. Plasma Science **16**, 90 (1988).
10. K.D. Pendergast, B.G. Danly, R.J. Temkin, and J.S. Wurtele, IEEE Trans. Plasma Science **16**, 122 (1988).
11. C. Chen and J.S. Wurtele, Phys. Rev. **A40**, 489 (1989).
12. N.M. Kroll, P.L. Morton, and M.N. Rosenbluth, IEEE J. Quantum Electron. **QE-17**, 1436 (1981).
13. L.R. Barnett, L.H. Chang, H.Y. Chen, K.R. Chu, W.K. Lau, and C.C. Tu, Phys. Rev. Lett. **63**, 1062 (1989), and references therein.
14. See, for example, *High Power Microwave Sources*, edited by V.L. Granatstein and I. Alexoff (Artech House, Boston, 1987), p. 397.
15. C. Chen and J.S. Wurtele, in preparation (1990).

FIGURE CAPTIONS

Fig. 1 The rf power in the TE_{11} and TE_{12} modes is plotted as a function of

interaction length z for (a) single-mode CARM interactions and (b) the CARM interaction with the coupled modes. Note in Fig. 1(b) that the TE_{12} mode grows parasitically with the dominant unstable TE_{11} mode at the same spatial growth rate due to mode coupling, despite the differences in launching losses.

Fig. 2 The TE_{12} rf power is plotted as a function of interaction length for a CARM with the TE_{11} and TE_{12} modes coupling to the beam. Here, the two solid curves depict the linear and nonlinear evolution of rf power for the TE_{12} mode obtained from the simulations with two input rf power distributions: (a) $P_0(TE_{11}) = 1.0$ kW and $P_0(TE_{12}) = 1.0$ kW, and (b) $P_0(TE_{11}) = 1.0$ kW and $P_0(TE_{12}) = 1.0$ W, while the two dashed curves are the corresponding analytical results from Eq. (6).

Fig. 3 The fractional rf power at saturation in four coupled TE_{1n} modes is plotted as a function of detuning. Here, the values of the resonant magnetic field for the TE_{11}, TE_{12}, TE_{13}, and TE_{14} modes correspond to $B_0 = 3.74$, 4.29, 5.33, and 6.98 kG, respectively.

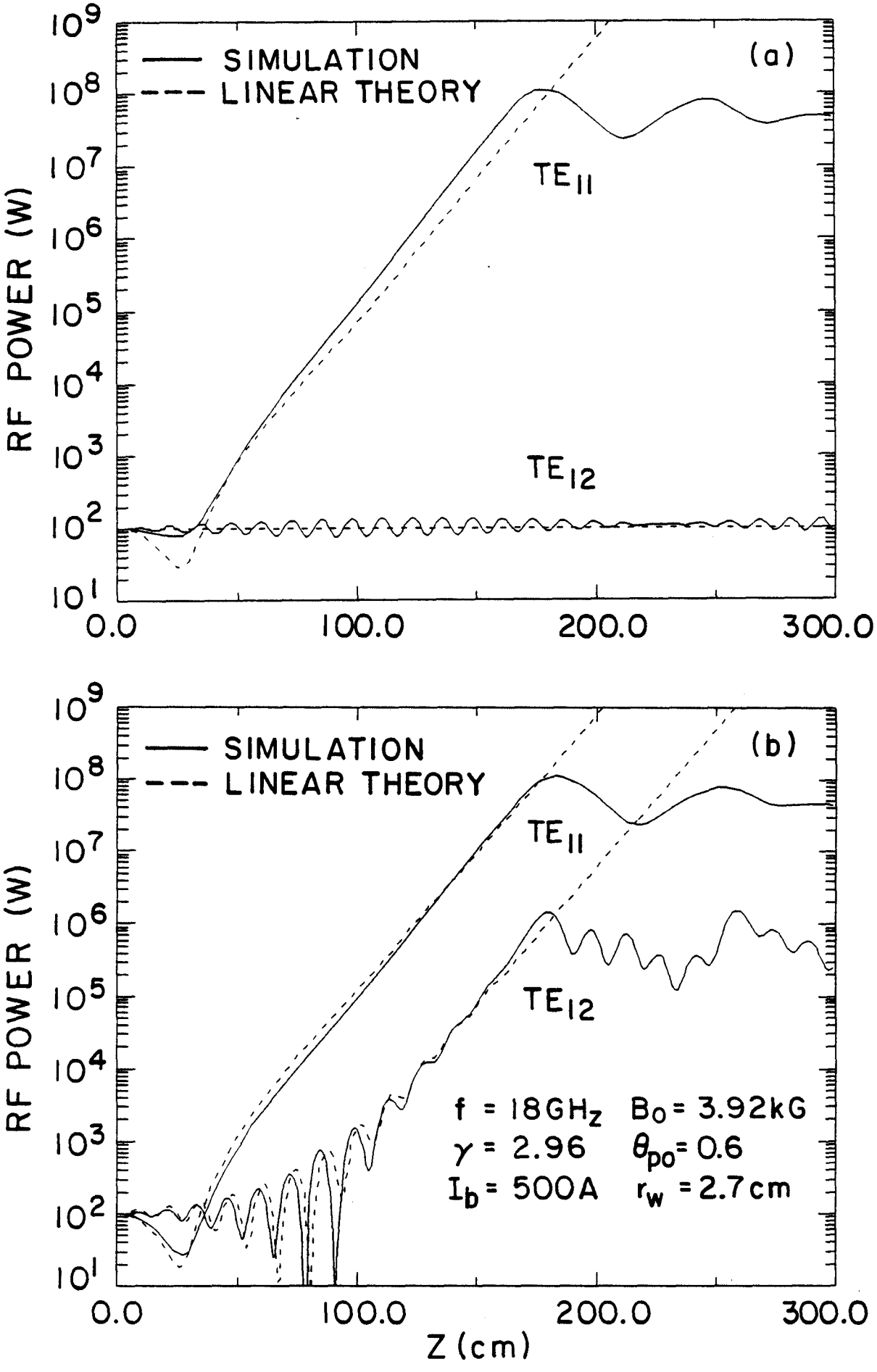
SIMULATION
LINEAR THEORY
(a)
TE11
TE12
RF POWER (W)
10^9
10^8
10^7
10^6
10^5
10^4
10^3
10^2
10^1
0.0
100.0
200.0
300.0
SIMULATION
LINEAR THEORY
(b)
TE11
TE12
f = 18GHz B0 = 3.92kG
γ = 2.96 θpo = 0.6
Ib = 500A rw = 2.7cm
RF POWER (W)
Z (cm)

Fig. 1

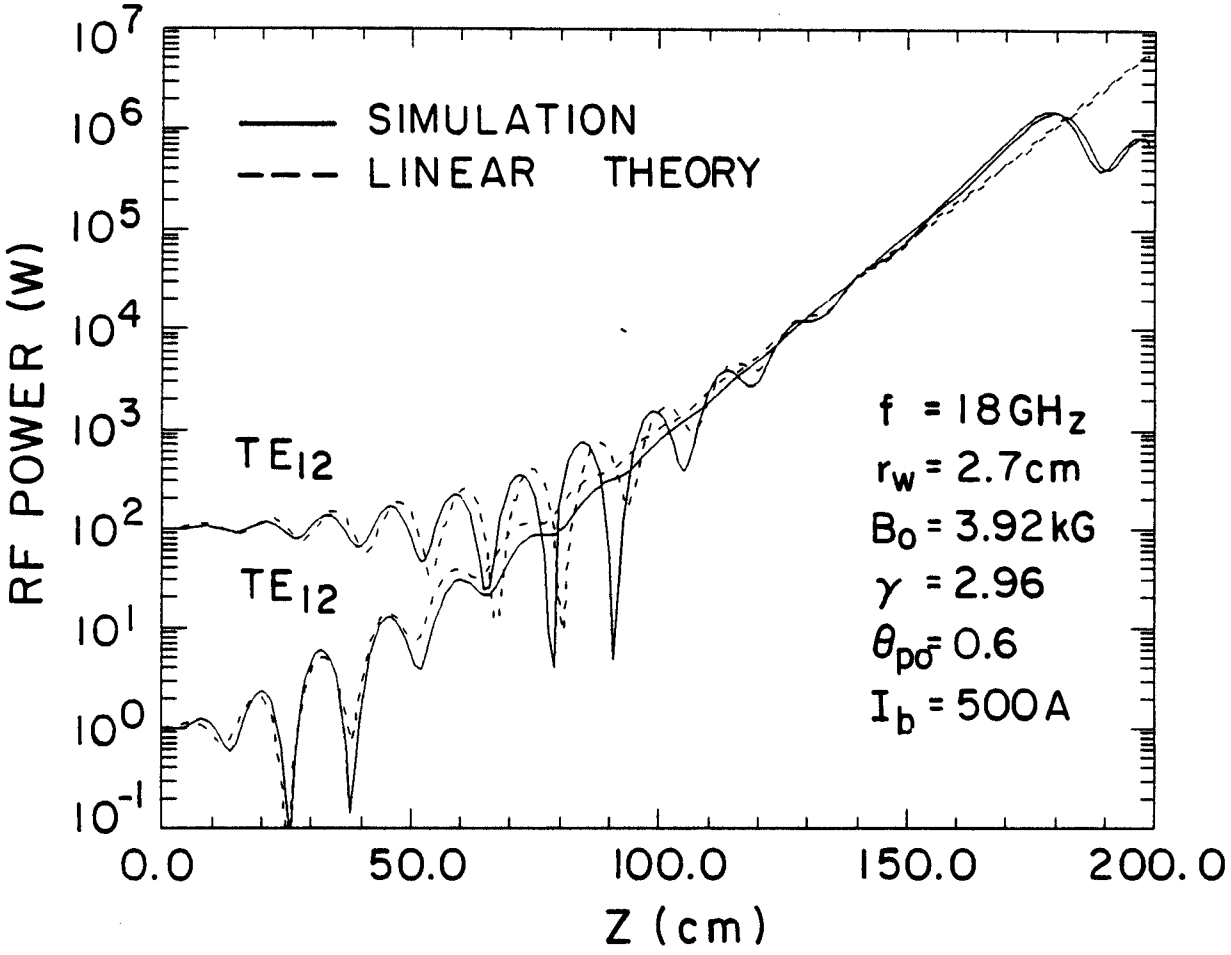
SIMULATION
LINEAR THEORY
TE12
TE12
f = 18GHz
rw = 2.7cm
Bo = 3.92kG
γ = 2.96
θpo = 0.6
Ib = 500A
RF POWER (W)
Z (cm)
10^7
10^6
10^5
10^4
10^3
10^2
10^1
10^0
10^-1
0.0
50.0
100.0
150.0
200.0

Fig. 2

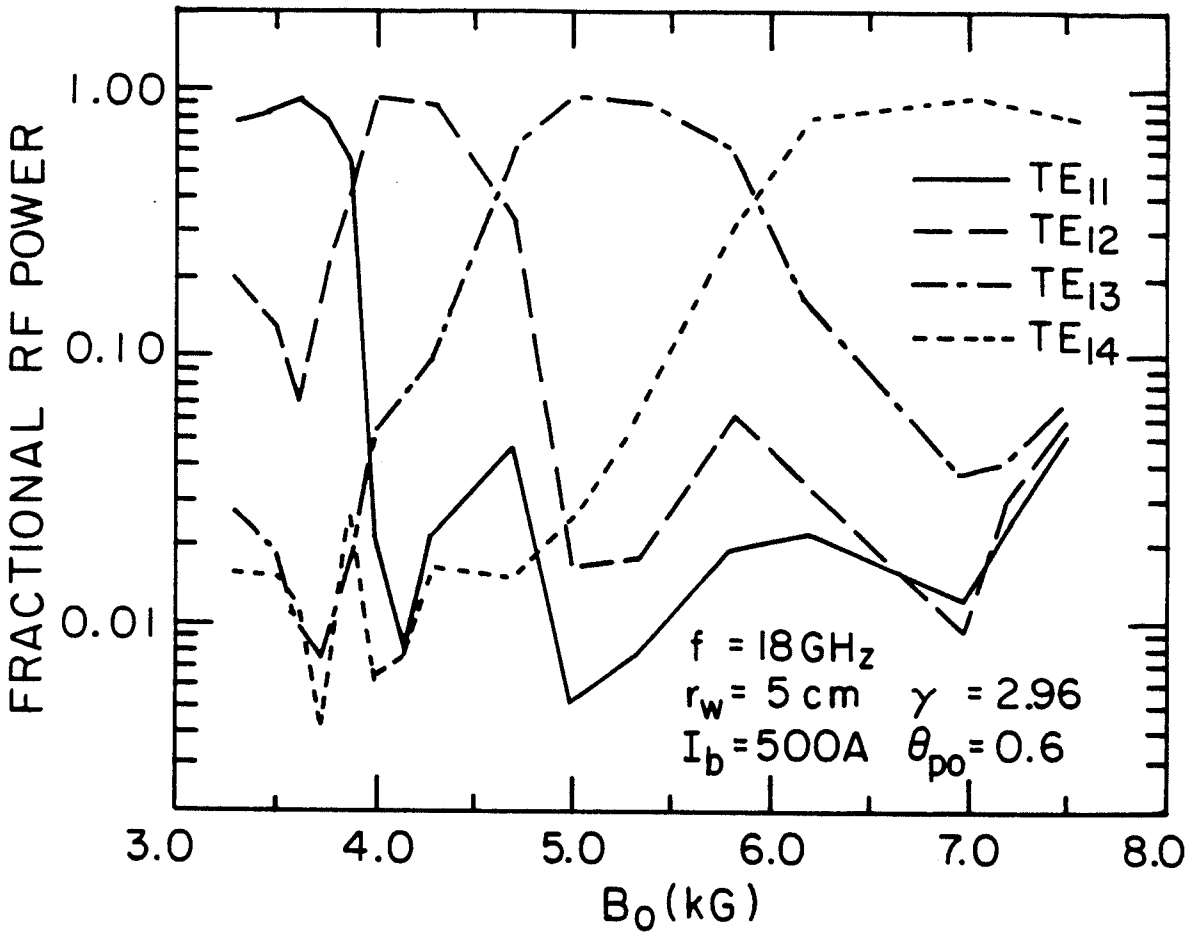
FRACTIONAL RF POWER
1.00
0.10
0.01
3.0
4.0
5.0
6.0
7.0
8.0
B_0(kG)
TE_{11}
TE_{12}
TE_{13}
TE_{14}
f = 18GHz
r_w = 5 cm
γ = 2.96
I_b = 500A
θ_{po} = 0.6

Fig. 3